Engineering Applications of Computational Fluid Mechanics Vol. 4, No. 3, pp. 374–386 (2010)

INFLUENCE OF BLUFF-BODY AND SWIRL ON MIXING AND INTERMITTENCY OF JETS

K.K.J. Ranga Dinesh*+, K. W. Jenkins*, A. M. Savill* and M. P. Kirkpatrick**

** School of Engineering, Cranfield University, Cranfield, Bedford, MK43 0AL, UK.*
+ E-Mail: Ranga.Dinesh@Cranfield.ac.uk (Corresponding Author)
*** School of Aerospace, Mechanical and Mechatronic Engineering, The University of Sydney, Sydney, NSW 2006, Australia*

ABSTRACT: In this paper we present the modelled results of turbulence, scalar mixing and intermittency for three different basic fluid dynamical problems using large eddy simulation (LES). The modelled problems are a turbulent round jet, a bluff body stabilised jet, and a bluff body stabilised swirl jet in a co-flow environment. Both instantaneous and time averaged results along with the probability density functions (pdf) and intermittency of velocity and passive scalar are presented. Simulations well captured the flow features of jet, bluff body stabilised jet and bluff body stabilised swirl jet. The instantaneous and time averaged data show the differences in turbulence and mixing and also an improvement of mixing in the presence of a bluff body and swirl. The addition of bluff body and swirl affect the structure of pdfs for both velocity and passive scalar at different axial and radial locations. The radial variation of intermittency at locations close to the centreline indicates turbulent to non-turbulent phenomena with respect to bluff body and swirl at both upstream and downstream recirculation regions.

Keywords: jet, bluff body, swirl, mixing, intermittency, LES

1. INTRODUCTION

The investigations of turbulence and mixing in engineering applications are continuously growing for a wide range of engineering and scientific applications in energy, environment, biological sciences etc. Theoretical, experimental and numerical studies of scalar mixing for benchmark fluid dynamical problems such as jet, coaxial jet, coaxial swirl jet etc. in confined and unconfined environment continue to be undertaken with the aim of improving the efficiency and accuracy of the mixing patterns while improving the safety and economy of associated engineering systems.

Early experimental investigations mainly focused on turbulent mixing of both reacting and non-reacting jet flows. For example, Corrsin (1943), Corrsin and Uberoi (1950) studied turbulent mixing and temperature fluctuations in turbulent jets. The turbulent quantities of the scalar field were also investigated by Oboukhov (1949), Corrsin (1951), Batchelor et al. (1959). Wygnanski and Fiedler (1969) demonstrated the details of turbulence intermittency and skewness for a self preserving jet. In addition, more recent experimental studies carried out by Panchapakesan and Lumley (1993), Hussein et al. (1994) and Dowling and Dimotakis (1990) demonstrated key physical aspects of turbulent mixing and statistical properties for turbulent axisymmetric jets.

Many experimental investigations also studied the self-similarity of a passive scalar. For example, Becker et al. (1967), Birch et al. (1978), Dahm and Dimotakis (1985) and Dowling and Dimotakis (1990) studied the self-similar behaviour of jets. Scheffer et al. (1994) also studied the large scale structure in a mixing of isothermal turbulent methane jet and analysed the instantaneous concentration profiles aiming for intermittency predictions. Warhaft (2000) reviewed the passive scalar mixing in turbulent flows and discussed many important aspects of the associated fluid dynamics such as energy spectra, probability density functions and variance. Various researchers also derived mathematical models for scalar mixing and applied them to different scalar mixing problems. For example, Broadwell and Breidenthal (1982) derived a mixing model based on flamelets and Kolmogorov cascade phenomena that can address jet flame blowout. Kerstein (1990) developed a powerful linear eddy model that can address the effects of Reynolds, Schmidt and Damkoeler number. The recent developments of computing hardware and software accessories now allow computational modellers to perform high fidelity numerical calculations with good degree of accuracy. Hence in recent time researchers have

Received: 27 Jul. 2009; Revised: 15 Mar. 2010; Accepted: 22 Mar. 2010

been keen to conduct high fidelity large scale numerical simulations such as so called direct numerical simulations (DNS) and large eddy simulations (LES). In DNS, all length and time scales of turbulence are directly resolved and hence no turbulence models are required, but currently this technique is only feasible for relatively low Reynolds number flows. In LES, large scales of turbulence are directly computed with the effect of the small scales requiring a turbulence model.

Recently several DNS studies have been carried out to study the scalar mixing in transitional and turbulent situations. For example, Brancher et al. (1994), Verzicco and Orlandi (1994) performed DNS of a transitional jet and Boersma et al. (1998) conducted DNS of a fully developed jet. Lubbers et al. (2001) extended Boersma's work and studied the self-similarity of the passive scalar field using DNS. Babu and Mahesh (2005) also investigated the passive scalar mixing for a turbulent jet using DNS and introduced a diffusive dominant brush-like region for a turbulent round jet.

However, the majority of DNS studies are still limited to moderate Reynolds number flows and hence investigators are keen to perform less expensive numerical simulations while maintaining good degree of accuracy. In this context, the large eddy simulation (LES) technique can be used for simulation of turbulent mixing especially for high Reynolds number flow situations. LES is capable of simulating higher Reynolds number flows in both simple and complex geometries and hence many calculations have been conducted successfully using affordable computing power.

Akselvoll and Moin (1996), for example, first computed mixing of turbulent confined coaxial jets using LES and compared their results with available experimental data. Pierce and Moin (1998) subsequently extended Akselvoll and Moin (1996) work for the coaxial swirl jet and conducted combustion calculations with heat release. Recently, Dianat, et al. (2006) studied the scalar mixing of a confined coaxial jet using LES and discussed different numerical schemes for the discretisation of scalar transport equation. Garcia-Villalba et al. (2006) discussed the large scale coherent structures in the near field of a confined coannular swirl jet. Very recently, Frohlich et al. (2008) also studied the scalar mixing and coherent structures for a coaxial swirl jet using LES.

The majority of investigations reported earlier were concerned mostly with a single problem such as a jet, a coaxial jet or a coaxial swirl jet. A detailed discussion of similarities and discrepancies for mixing and intermittency within a single framework has not been pursued. The discussion of such work in a single framework is particularly needed to achieve greater universality in engineering problems while improving the overall understanding of such problems. To this end the present work uses LES to study the turbulence, mixing and intermittency of three different benchmark problems within a single framework. The problems considered for this work may be defined as a turbulent jet, a bluff body stabilised jet, a bluff body stabilised swirl jet.

In this work, first we address the similarities and differences for both velocity and scalar fields to ensure that the LES subgrid model along with numerical discretisation schemes reliably predict the different flow features and scalar mixing patterns and then discuss the probability density functions and intermittency profiles for relevant configurations. The remainder of the paper is organised as follows: in section 2, we discuss the details of three different configurations. In section 3, we describe the governing equations and modelling followed by the numerical setup. Section 4 discusses the results from these simulations and finally the conclusion is given in section 5.

2. DETAILS OF THE MODELLED GEOMETRIES

Figure 1 shows schematics of the three problems considered in this work. The round jet has a diameter of D=3.6mm and the same diameter is used for the jet of the bluff body stabilised case and the bluff body stabilised swirl case. The diameter of the bluff body is chosen as 50mm. For the bluff body stabilised swirl jet, a secondary annulus with 60mm diameter is used. All three cases also use a secondary axial co-flow. The flow parameters are the bulk axial velocity of the jet, U_j, bulk axial and tangential velocities of the annular stream, U_s and W_s, and the co-flow velocity of the secondary stream, U_e. The Reynolds number of the jet is defined in terms of the primary (bulk) axial velocity (66 m/s), the diameter of the jet (D=3.6mm) and the kinematic viscosity of air ν such that $\mathrm{Re}_j = U_j D/\nu$. The geometric swirl number (S_g) is expressed as the ratio of integrated (bulk) tangential velocity to

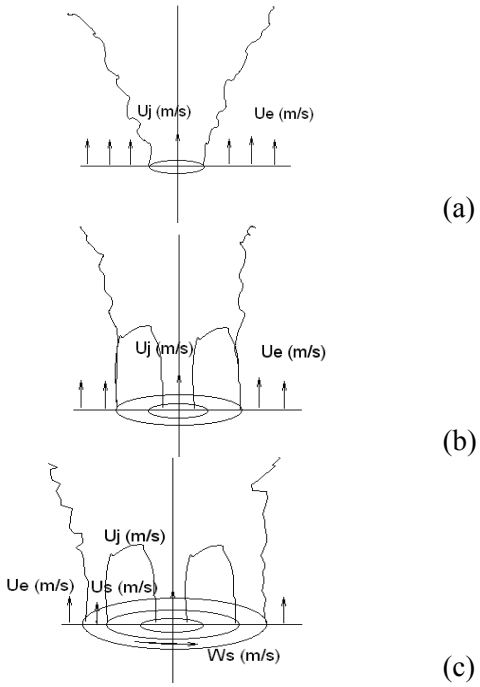

Fig. 1 Configurations used for the present study. The jet diameter is 3.6mm, the bluff body diameter is 50mm and the swirling annulus diameter is 60mm respectively.

primary axial air velocities (W_s/U_s). The Schmidt number used is $\sigma = 0.7$. Table 1 shows the values of the flow parameters used in the present work.

3. COMPUTATIONAL SETUP

3.1 Mathematical formulations

The LES technique is based on the explicit simulation of the largest scales, whilst the effect of the smaller scales (the so called sub-grid scales) are modelled using a sub-grid scale (SGS) model. The governing equations are the spatially filtered incompressible mass, momentum and passive scalar equations and can be written as:

$$\frac{\partial \overline{u}_j}{\partial x_j} = 0 \tag{1}$$

$$\frac{\partial \overline{u}_i}{\partial t} + \frac{\partial (\overline{u}_i \overline{u}_j)}{\partial x_j} = -\frac{1}{\rho}\frac{\partial \overline{P}}{\partial x_i} + \frac{\partial (2\nu \overline{S}_{ij})}{\partial x_j} - \frac{\partial (\tau_{ij})}{\partial x_j} \tag{2}$$

$$\frac{\partial \overline{f}}{\partial t} + \frac{\partial (\overline{u}_j \overline{f})}{\partial x_j} = (\frac{\nu}{\sigma})\frac{\partial^2 \overline{f}}{\partial x_j \partial x_j} - \frac{\partial \gamma}{\partial x_j} \tag{3}$$

where $u_i, \rho, p, v, f, \sigma$ denote the velocity, density, pressure, kinematic viscosity, passive scalar concentration and laminar Schmidt numbers, and the strain rate tensor, $S_{ij} = \frac{1}{2}\left(\frac{\partial \overline{u}_i}{\partial x_j} + \frac{\partial \overline{u}_j}{\partial x_i}\right)$.

The terms $\tau_{ij} = \left(\overline{u_i u_j} - \overline{u}_i \overline{u}_j\right)$ in equation (2) and $\gamma = (\overline{u_j f} - \overline{u}_j \overline{f})$ in equation (3) result from the unresolved sub-grid scale contributions and hence subsequent modelling is required to close the filtered momentum equations and filtered scalar equation. Here we employed the Smagorinsky (1963) eddy viscosity model to calculate the SGS stress tensor $\tau_{ij} = \left(\overline{u_i u_j} - \overline{u}_i \overline{u}_j\right)$ such that

$$\tau_{ij} - \frac{1}{3}\delta_{ij}\tau_{kk} = -2\nu_{sgs}\overline{S}_{ij} \tag{4}$$

$$\gamma = \frac{-\nu_{sgs}}{\sigma_t}\frac{\partial \overline{f}}{\partial x_j} \tag{5}$$

where σ_t is the turbulent Schmidt number. Here the eddy viscosity ν_{sgs} is given as a function of the filter size and strain rate

$$\nu_{sgs} = C_s \overline{\Delta}^2 \left|\overline{S}\right| \tag{6}$$

Table 1 Flow conditions used in the study.

Flow case	U_s(m/s)	W_s(m/s)	U_j(m/s)	U_e (m/s)	S_g	Re_j
Jet	0.0	0.0	66	20	0	14000
Bluff body stabilised jet	0.0	0.0	66	20	0	14000
Bluff body stabilised swirl jet	29.7	16.0	66	20	0.54	14000

where C_s is a Smagorinsky (1963) model parameter and $|\overline{S}| = (2\overline{S}_{ij}\overline{S}_{ij})^{\frac{1}{2}}$. Here we employed the localised dynamics procedure of Piomelli and Liu (1995) to obtain the subgrid scale turbulent Schmidt number (σ_t) and the model parameter C_s appearing in equations (5) and (6).

3.2 Numerical discretisation

The mathematical formulations for mass, momentum and passive scalar are numerically solved by means of a pressure based finite volume method using the large eddy simulation code PUFFIN developed by Kirkpatrick et al. (2003a, b) and validated for a wide range of applications including reacting and non-reacting swirl flows (Ranga-Dinesh and Kirkpatrick, 2009, Kempf et al. 2008). The code has been recently parallelised by Kirkpatrick (2008) and the results presented in this paper have been obtained using the parallel version. Spatial discretisation is achieved using a non-uniform Cartesian grid with a staggered cell arrangement. Second order central differences (CDS) are used for the spatial discretisation of all terms in both the momentum equation and the pressure correction equation. This minimises the projection error and ensures convergence in conjunction with an iterative solver. The diffusion terms of the passive scalar transport equation are also discretised using the second order CDS. The convection term of the passive scalar transport equation is discretised using a third order QUICK with ULTRA flux limiter (Leonard, 1990) to ensure that the solution remains monotonic.

The momentum and passive scalar transport equations are integrated in time using a second order Adams-Bashforth scheme. The pressure correction method of Van Kan (1986) and Bell et al. (1989) which involves solving an equation for pressure correction rather than the pressure is used for the present work. The solution to this equation is then used to project the approximate velocity field that results from the integration of the momentum equations onto a subset of divergence free velocity fields. The time step is varied to ensure that the maximum Courant number $C_o = \Delta t u_i / \Delta x_i$ remains approximately constant where Δx_i is the cell width, Δt is the time step and u_i is the velocity component in the x_i direction. The solution is advanced with time steps corresponding to a Courant number in the range of $C_o = 0.3$ to 0.5. A Gauss-Seidel solver is used to solve the system of algebraic equations resulting from the numerical discretisation of momentum and passive scalar transport equations. The BiCGStab method with a Zebra Gauss-Siedel preconditioner using successive overrelaxation (SOR) and Chebyshev acceleration is used to solve the algebraic equations resulting from the discretisation of pressure correction equation.

3.3 Domain size, grid resolution and boundary conditions

The computations were performed on a non-uniform Cartesian grid in a domain with dimensions $300 \times 300 \times 250mm$. The grid has $160 \times 160 \times 120$ cells in the *x*, *y* and *z* directions respectively giving a total of approximately three million cells. Grid lines in the *x* and *y* directions use an expansion ratio of $\gamma_{xy} = \Delta x(i)/\Delta x(i-1) = 1.05$ and an expansion ratio of $\gamma_z = 1.03$ is used in the z-direction. The mean velocity distributions for the jet and annulus flows were specified using power law velocity profiles such as:

$$< U >= 1.218 U_j \left(1 - \frac{|y|}{\delta}\right)^{1/7} \qquad (7)$$

where U_j is the bulk velocity, y the radial distance from the jet centre line and $\delta = 1.01 r_j$, where $r_j = 1.8mm$. Similar format is used for the primary annulus to specify the mean axial and swirl velocities by replacing corresponding parameters. The turbulence at the inlets is modelled by superimposing fluctuations on the mean velocity profiles generated from a Gaussian distribution. A top-hat profile is used as the inflow conditions for the passive scalar. A free slip boundary conditions is applied at the solid walls and at the outflow plane, a convection boundary condition is used for the velocities and a zero normal gradient is used for the passive scalar. All simulations were carried out for the total time period of 300*ms* and two non-consecutive sampling periods yielded similar results indicating that the statistics were well converged.

4. RESULTS AND DISCUSSION

The results will be discussed under two sections. The basic idea of the separation is to discuss the mean flow calculations and intermittency separately. The first section discusses the velocity field for both instantaneous and time averaged quantities and the second section discusses the

probability density functions (pdf) and radial variation of intermittency for both velocity and scalar fields.

4.1 Instantaneous and Mean Flow Calculations

Figures 2(a-c) show instantaneous velocity vectors for the jet, bluff body stabilised jet, and bluff body stabilised swirl jet. The plots show an increase in the complexity of the vector field for the bluff body stabilised jet and the bluff body stabilised swirl jet. The velocity vector field for the jet is noticeably different from the other two cases. It remains almost parallel in the near field which is affected by the co-flow velocity and decays smoothly at downstream axial locations. However, the velocity field with a bluff body (Figure 2(b)) shows vortex roll up in the near field and the formation of a recirculation zone due to the adverse pressure gradient. The bluff body stabilised jet (Figure 2(b)) also expands radially at a significantly greater rate than that seen for the jet (Figure 2(a)). In the bluff body stabilised swirl jet (Figure 2(c)), the swirl causes rapid axial momentum decay and also creates more rotational vortices in the near field and far field regions. These rotational vortices interact with the swirl velocities and form complex flow patterns (Figure 2(c)). The velocity vector field in the swirl case also shows different vorticity structures in the central region which indicate a high level of turbulence in the regions where we can expect precession behaviour.

Figures 3(a-c) show the contour plots of the time averaged mean axial velocities for the three cases. As seen in Figure 3(a) the calculation well captured the centre jet potential core while observing the axisymmetric behaviour. Figure 3(b) shows the bluff body stabilised recirculation zone and the formation of counter rotating vortices associated with the jet and co-flow which are identical at both sides of the jet. A torroidal shaped recirculation zone is formed as a result of sudden expansion at the bluff body wall. However, there is no stagnation point along the centreline. No lateral spread is being imposed onto the central jet by the recirculation zone. The centre jet potential core has been significantly reduced as a result of the bluff body and therefore the centreline axial velocity reduces compared with the plain jet. Figure 3(c) shows the time averaged mean axial velocity for the bluff body stabilised swirl jet. As expected, the flow field exhibit complex flow patterns involving the formation of a second centre recirculation zone known as a vortex breakdown (VB) bubble. In the swirl case, the formation of the upstream recirculation zone is different from that of the bluff body and the size of the eddies inside the upstream recirculation zone are relatively smaller than that in the bluff body stabilised jet, which is directly affected by the primary annulus velocities. In addition, the momentum of the annular jet moves more rapidly away from the centreline demonstrating that the jet spreads more rapidly depending on the local strength of the swirl.

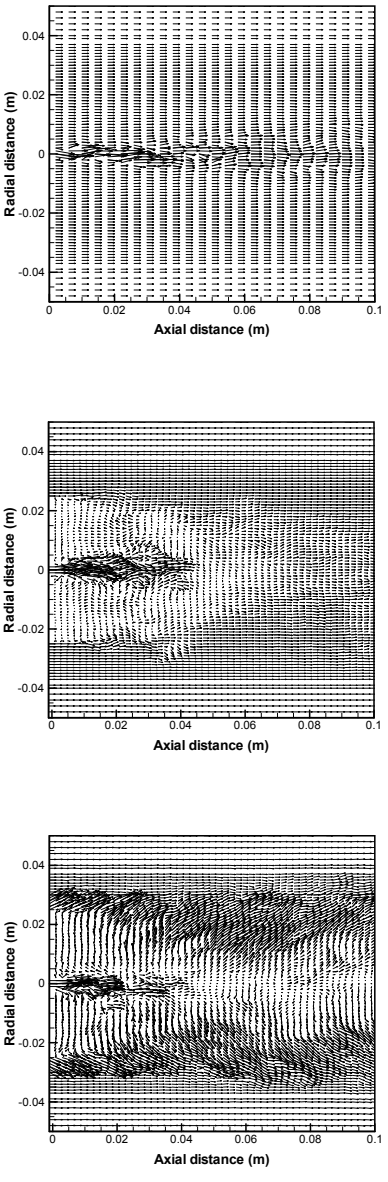

Fig. 2 Instantaneous velocity vector fields for (a) jet, (b) bluff body stabilised jet and (c) bluff body stabilised swirl jet.

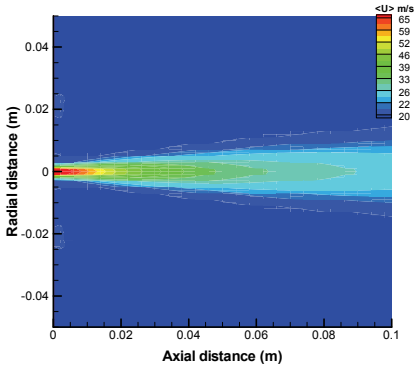

(a)

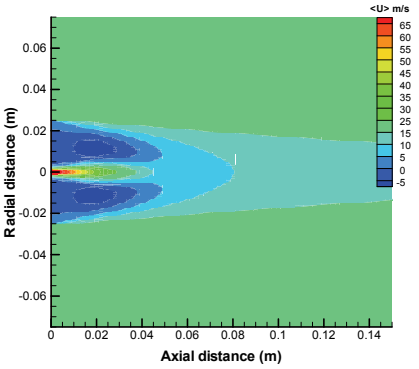

(b)

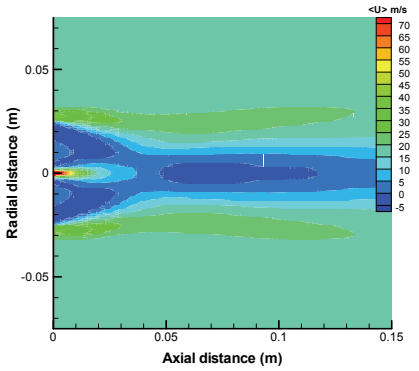

(c)

Fig. 3 Contour plots of the mean axial velocity for (a) jet, (b) bluff body stabilised jet and (c) bluff body stabilised swirl jet.

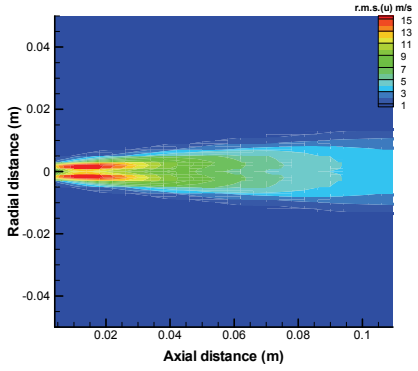

(a)

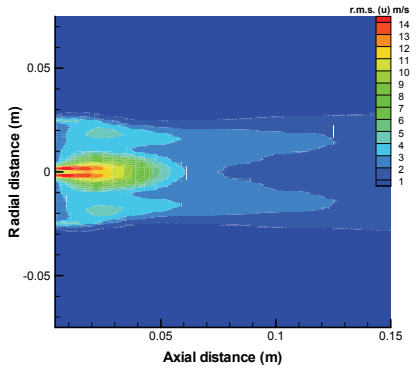

(b)

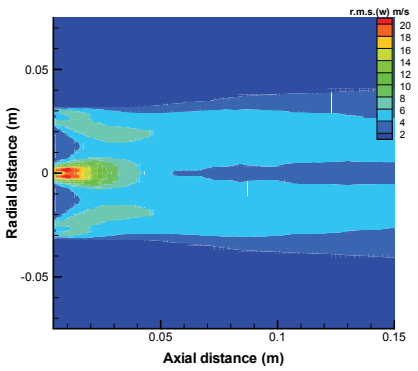

(c)

Fig. 4 Contour plots of the r.m.s. axial velocity for (a) jet, (b) bluff body stabilised jet and (c) bluff body stabilised swirl jet.

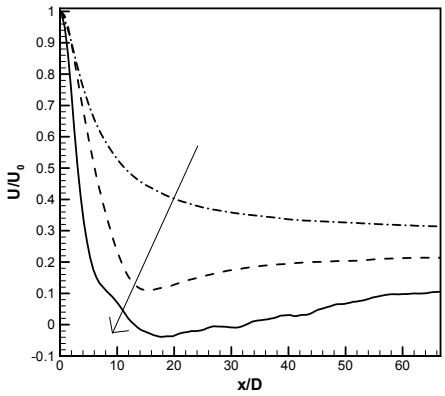

Fig. 5 Centreline mean axial velocity. Chained, dashed and solid lines indicate results for the jet, bluff body stabilised jet and bluff body stabilised swirl jet, respectively.

Figures 4(a-c) show the root mean square (r.m.s) fluctuations of axial velocity. The rms axial fluctuation of the plain jet (Figure 4(a)) has high values in the shear layer region and gradually decreases in the far field. For the bluff body stabilised jet (Figure 4(b)), high rms axial fluctuations are observed in regions where the centre jet is constrained by the recirculating flow. The rms axial fluctuations for Figure 4(b) and (c) contain anisotropy of turbulence inside recirculation zones and the present simulations accurately captured the turbulence structures for the two cases. It may also be observed that the rms fluctuations remain relatively high inside the recirculation region while mean axial velocities are small.

The time averaged centreline mean axial velocity is shown in Figure 5. The plot shows the scaled centreline velocity U/U_0 as a function of the distance from the jet exit plane (here U m/s is the centreline axial velocity and U_0 is the axial velocity at jet orifice). As seen in this figure, the reduction of the mean axial velocity along the centreline is clearly visible for both bluff body stabilised and bluff body stabilised swirl jets. The sudden reduction of the mean axial velocity appears in between x/D=10-20 in where the bluff body stabilised recirculation forms. In addition, the swirl jet shows a negative mean axial velocity and thus forms the vortex breakdown bubble. In earlier studies, we have shown that LES results and in good agreement with experimental data for both bluff body stabilised jet and bluff body stabilised swirl jet and complete discussion can be found in Malalasekera et al. (2007).

Figures 6-8 show the iso-surfaces of the passive scalar for the jet, bluff body stabilised jet and bluff body stabilised swirl jet respectively. Such information provides a good insight into the development of the passive scalar field over the computational domain. The iso-surface for the jet expands uniformly through the domain. The iso-surfaces of the bluff body stabilised jet shows more rapid expansion in the radial direction and appears to be more strongly affected by turbulence structures from the bluff body. The turbulence and mixing expand radially even more rapidly in the bluff body stabilised swirl jet as a result bluff body and swirl. Hence the bluff body stabilised swirl jet shows more turbulence structures at both upstream and downstream recirculation regions. Finally, these plots indicate how mixing takes place for three different situations.

Figure 9 shows the instantaneous passive scalar in a plane perpendicular to the axial direction (cross section) at x/D=10 downstream axial location. Here D is the diameter of the jet (D=3.6mm). The selected axial location lies within the bluff body stabilised recirculation zone and hence we are able to analyse the effect of the recirculation zone on scalar mixing. Figure 9(a), (b) and (c) shows the snapshots of passive scalar for the jet, bluff body stabilised jet and bluff body stabilised swirl jet. As seen in Figure 9(a) the radial expansion of the jet is very small. However the recirculation zone directly acts to spread the scalar and thus improves the mixing for the bluff body stabilised jet and bluff body stabilised swirl jet. Furthermore, swirl does not appear to improve the mixing in the upstream recirculation region which is mainly dominated by the bluff body stabilised recirculation zone.

Figure 10 shows the velocity vector field and passive scalar at a cross section of the jets at x/D=20. Figure 10(a) and (b) shows the velocity vector field and instantaneous passive scalar for

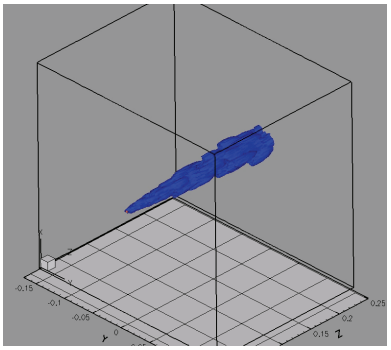

Fig. 6 Iso-surfaces of the passive scalar for jet for a value of 0.05.

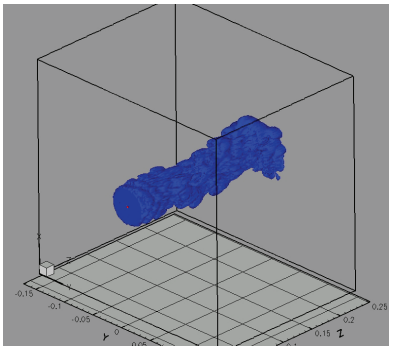

Fig. 7 Iso surfaces of the passive scalar for a bluff body stabilised jet for a value of f=0.05.

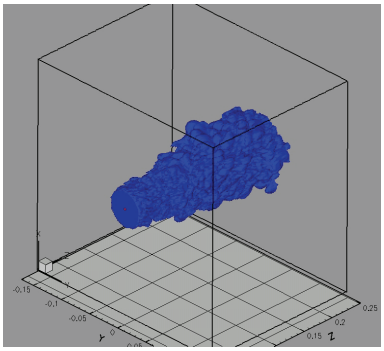

Fig. 8 Iso-surfaces of the passive scalar for a bluff body stabilised swirl jet for a value of f=0.05.

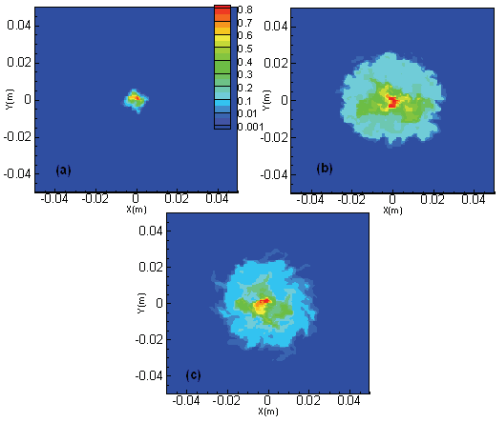

Fig. 9 Instantaneous passive scalar in cross section at x/D=10. Here (a) jet, (b) bluff body stabilised jet and (c) bluff body stabilised swirl jet.

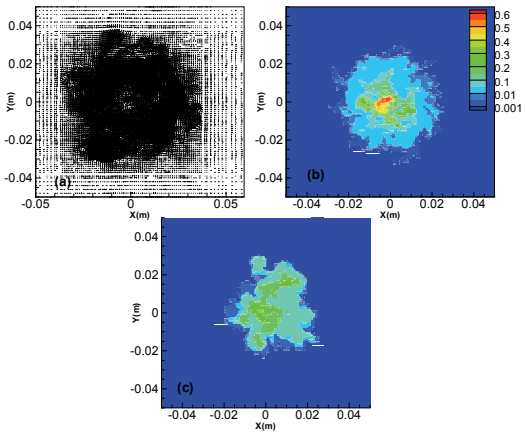

Fig. 10 Comparison of the (a) velocity vector field, (b) instantaneous passive scalar field for bluff body stabilised swirl jet and (c) bluff body jet at x/D=20.

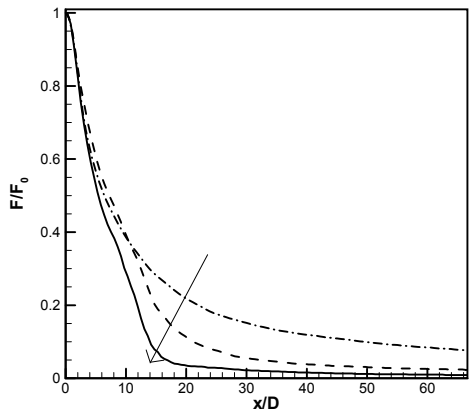

Fig. 11 Centreline mean passive scalar, chained, dashed and solid lines indicate results for the jet, bluff body stabilised jet and bluff body stabilised swirl jet, respectively.

bluff body stabilised swirl jet while (c) shows the passive scalar mixing for the bluff body stabilised jet at x/D=20 where the swirl induced second downstream recirculation occurs. The velocity vector field shows the occurrence of rotational vortices while passive scalar mixing (b) shows improvement of radial spread as a result of the swirl. However passive scalar mixing (c) of bluff body stabilised jet shows less mixing and less radial spread due to the absence of swirl induced recirculation zone. Therefore figures 9 and 10 shows how bluff body individually and in combination with swirl affect the temporal evolution of the scalar mixing inside the recirculation zones created by bluff body and swirl.

Figure 11 shows the axial decay of the mean centreline passive scalar scaled with the values at the orifice. Here F is the centreline passive scalar and F_0 is the passive scalar value at jet orifice, and D is the diameter of the jet (3.6mm). The plots contain three data sets such that the chained, dashed and solid lines indicate results for the jet, bluff body stabilised jet and bluff body stabilised swirl jet respectively. The passive scalar of the jet, bluff body stabilised jet and bluff body stabilised swirl jet profiles collapse to one curve at near field and then start to diverge from each other at intermediate and far field axial locations. As indicated by the arrow in Figure 11 the centreline mean passive scalar starts to decrease at around x/D=15 which appears sharp for bluff body stabilised and swirl stabilised jets respectively. The effect of the bluff body cause a decrease of mean passive scalar by about a factor of two compared with the plain jet. In the swirl case, both bluff body and swirl together act to reduce the centreline mixing by approximately a factor of three compare to the jet only case. Therefore the combination of bluff body and swirl can significantly increase the mixing in the radial direction and thus reduce the axial extent of the high concentration zone.

Figures 12 and 13 show radial profiles of the time averaged mean passive scalar and passive scalar variance at six axial locations. The profiles were produced to cover the near field, intermediate region and far field axial locations. The plots contain three data sets such that the chained, dashed and solid lines indicate results for the jet, bluff body stabilised jet and bluff body stabilised swirl jet respectively. Figure 12 shows that the profiles at the first two axial locations indicate the radial spread of the passive scalar is very much

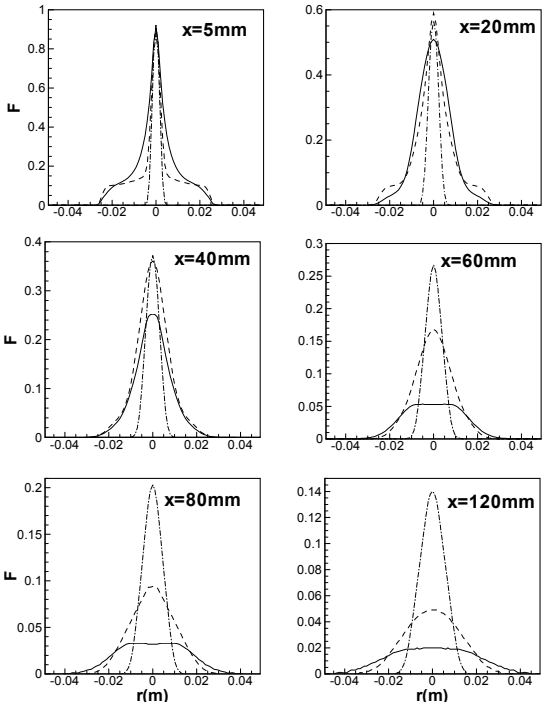

Fig. 12 Radial comparisons of mean passive scalar, chained, dashed and solid lines indicate results for the jet, bluff body stabilised jet and bluff body stabilised swirl jet, respectively.

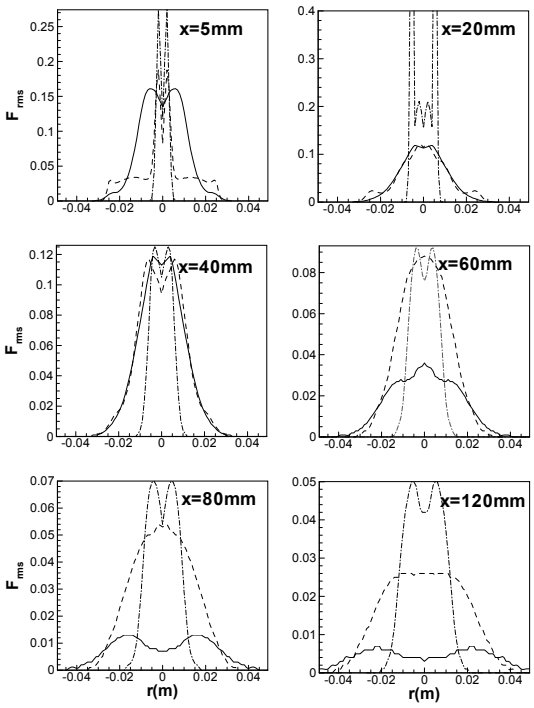

Fig. 13 Radial comparisons of passive scalar variance, chained, dashed and solid lines indicate results for the jet, bluff body stabilised jet and bluff body stabilised swirl jet, respectively.

similar for jets with bluff body and swirl. However, the difference becomes increasingly apparent at downstream axial locations as a result of vortex breakdown. Although the centreline mean axial velocity significantly reduces for the swirl case at downstream locations compared to the plain jet, the radial spread shows similar behaviour for the bluff body stabilised jet and bluff body stabilised swirl jet. Further downstream, the passive scalar is seen to mix much more rapidly in the swirl cases, due to direct effect of the VB bubble. Figure 13 shows radial profiles of the passive scalar variance at six different axial locations. The plots of the passive scalar variance show high peaks in the plain jet. The peaks are lower for the bluff body stabilised jet and bluff stabilised swirl jet.

4.2 Intermittency Calculation

The mathematical definition for intermittency can be expressed using an indicator function with the value of one in turbulent regions and zero in non-turbulent (laminar) regions. The indicator function represents a fraction of the time interval during which a point is inside the turbulent fluid. A normalised histogram method tested by Andreotti and Douady (1999) can be used to determine the probability density function (pdf) which is required for the intermittency calculation. Thus the intermittency value can be calculated using a summation of probability values for a given threshold value (it is important to note that we consider external intermittency i.e. at the interface between turbulent and non-turbulent zones rather than internal intermittency which refers to the variability of energy within the turbulent scales) .

In this study we used the method proposed by Schefer and Dibble (2001) for intermittency calculation. In this method, the intermittency can be calculated from pdfs in which we assumed that the pdf is smooth at the scale of one histogram bin. Here 8000 measurements at each spatial location with 50 bins over $3-\sigma$ limits of data are considered. Therefore the normalised pdf's can be written as

$$\int_0^1 P(f)df = 1 \tag{8}$$

The intermittency value γ (Gamma) can be calculated from the probability values respect to considered threshold value such that

$$\gamma = P(f > f_{th}) \tag{9}$$

The comparisons of velocity pdf distributions at equidistant radial locations r=0mm, 10mm, 20mm and 30mm at different axial locations x=40mm and x=100mm are presented in Figures 14 and 15. As seen in Figure 14(a) the evolution of the centreline velocity pdfs (r=0mm) at x=40mm follow more like a delta function for both jet and bluff body stabilised jet, while pdf of the bluff body stabilised swirl jet follows Gaussian distribution. The formation of an upstream recirculation zone affects the near field axial velocity and thus creates differences for the velocity pdfs at x=40mm for the three cases.

Particularly, the pdf shapes are less structured for both bluff body stabilised jet and bluff body stabilised swirl jet at intermediate radial locations (Figures 14(b) and (c)) before shift towards the delta function at far radial location (Figure 14(d)). Figure 15 shows the pdfs of velocity at further downstream axial location, x=100mm. The effects of the downstream centreline recirculation bubble on pdf velocity can also be seen for the bluff body stabilised swirl jet. Again, pdfs of both bluff body stabilised jet and bluff body stabilised swirl jets show Gaussian behaviour while jet results show delta function at near field radial locations (Figures 15(a) and (b)). However, all scalar pdf distributions for the three cases shift towards the delta function at far radial locations (r=20mm, 30mm) at downstream axial location x=100 (Figures 15(c) and (d)). It has been also observed that pdfs of the axial velocity show less structure at some radial locations due to frequent changes of the velocity fluctuations for both bluff body stabilised jet and bluff body stabilised swirl jet and thus indicate a sign of intermittency.

Figure 16 shows the radial profiles of velocity intermittency at x=40, 80, 100, 120mm. Since all three cases have a secondary co-flow velocity of 20 m/s, here we used the threshold value of $u_{th} = 15.0 m/s$. As expected, variations of the intermittency values indicate bluff body and swirl effects on velocity intermittency with respect to a selected threshold value. An occurrence of a recirculation zone due to a circular bluff body reduces the intermittency value on the centreline at near field axial locations (x=40mm) and thus indicates the changes from turbulent to non-turbulent phenomena. Moreover, an occurrence of downstream recirculation zone induced by swirl further reduces the intermittency values on the centreline at far field axial locations (x=100mm, 120mm). Although the velocity intermittency profiles are similar for the bluff body stabilised jet and the bluff body stabilised swirl jet inside the upstream first recirculation zone (Figure 16(a)) the difference largely occurs at further downstream (Figures 16(c) and (d)) due to the second swirl induced centre recirculation zone (x=100mm, 120mm). Therefore the radial velocity intermittency profiles show rapid variation with respect to formation of recirculation zones and thus provides useful details for the intermittent behaviour with respect to bluff body and swirl.

The probability density function (pdf) of a passive scalar at radial locations r=0mm, 10mm, 20mm and 30mm at two different axial locations x=40mm and x=100mm are shown in Figures 17 and 18. A similar approach to that discussed for velocity intermittency was again applied to determine the probability density functions of a passive scalar. As seen in Figure 17(a), the centreline pdf of the passive scalar show Gaussian shape for the bluff body stabilised swirl jet and delta function for the other two cases. Again pdfs become more irregular at intermediate axial locations for both bluff body stabilised jet and bluff body stabilised swirl jet and gradually becomes delta function at far radial locations (Figure 17(d)). However, as seen in Figure 18, pdfs of the passive scalar show more irregular behaviour close to the centreline for both bluff body and swirl jets at x=100mm (Figures 18(a) and (b)). This gives an indication about intermittency of scalar mixing near the centreline due to presence of one or more recirculation zones. The radial profiles of the passive scalar intermittency at x=40, 80, 100, 120mm are shown in Figure 19. Here we considered a threshold value of $f_{th} = 0.015$. Again the scalar intermittency profiles (Figures 19(c) and (d)) demonstrate the effect of swirl on scalar intermittency as the centreline scalar intermittency show changes from turbulent to non-turbulent inside the centre recirculation zone.

The present findings of the intermittency results indicate reasons for further development of LES based sub-grid models. Particularly, development of generic LES sub-grid models such as solving an additional modified intermittency transport equation with an appropriate sub-grid model would help to derive more generic model which could effectively tackle turbulence intermittency. In such case, an intermittency factor could simply be included in the Smagorinsky eddy viscosity model once determined from the intermittency transport equation.

5. CONCLUSIONS

The primary focus of this work was to examine

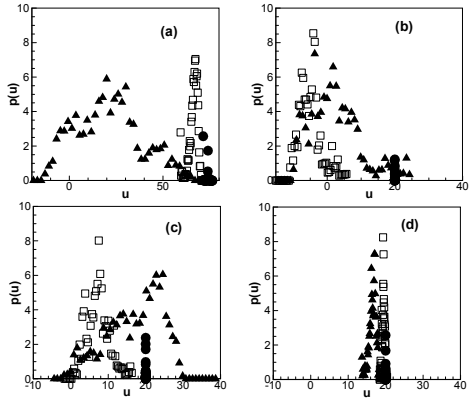

Fig. 14 Probability density function (pdf) of the axial velocity at x=40mm, circles, squares and triangles indicate results for the jet, bluff body stabilised jet and bluff body stabilised swirl jet, respectively.

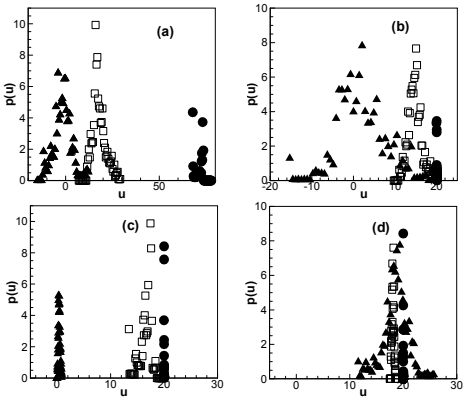

Fig. 15 Probability density function (pdf) of the axial velocity at x=100mm, circles, squares and triangles indicate results for the jet, bluff body stabilised jet and bluff body stabilised swirl jet, respectively.

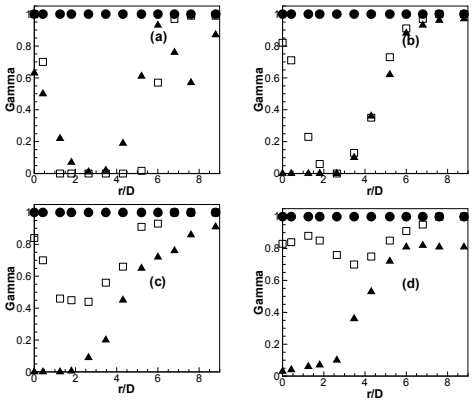

Fig. 16 Radial profiles of velocity intermittency at (a) x=40mm, (b) x= 80mm, (c) x=100mm and (d) x=120mm. Here, circles denote jet results, squares denote bluff body stabilised jet results and triangles denote body stabilised swirl jet results.

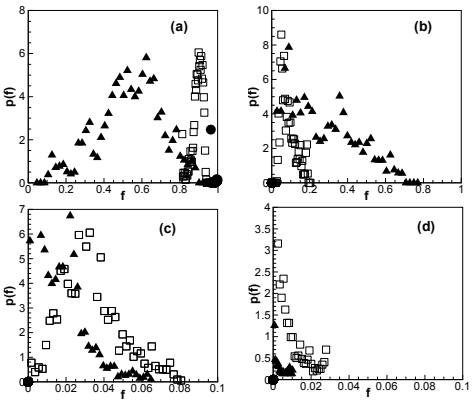

Fig. 17 Probability density function (pdf) of the passive at x=40mm. Here, circles, squares and triangles indicate results for the jet, bluff body stabilised jet and bluff body stabilised swirl jet, respectively.

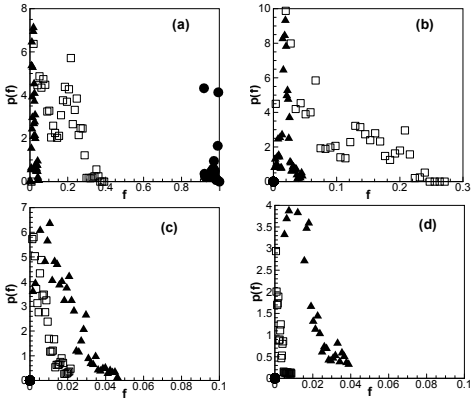

Fig. 18 Probability density function (pdf) of the axial velocity at x=100mm, circles, squares and triangles indicate results for the jet, bluff body stabilised jet and bluff body stabilised swirl jet, respectively.

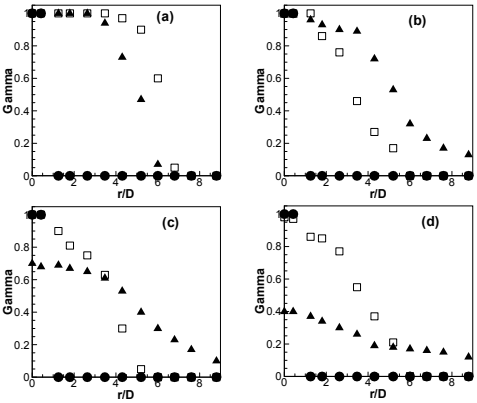

Fig. 19 Radial profiles of scalar intermittency at (a) x= 40mm, (b) x= 80mm, (c) x= 100mm and (d) x= 120mm. Here, circles denote jet results, squares denote bluff body stabilised jet results and triangles denote body stabilised swirl jet results.

turbulence, mixing and intermittency for three different benchmark problems using large eddy simulations. The modelled problems were the jet, bluff body stabilised jet, and bluff body stabilised swirl jet. The instantaneous and mean velocity fields for all three cases show the increase of complexity with the addition of bluff body and swirl. Derived probability density function distributions for both velocity and passive scalar indicate changes from Gaussian distributions to a delta function at selected axial and radial locations. The intermittency factors calculated at different axial locations demonstrate the regional changes between turbulent and laminar regimes with respect to a given threshold. The radial intermittency profiles further indicate differences at near and far field axial locations especially close to the jet centreline due to formation of one or more recirculation zones.

ACKNOWLEDGEMENT

We are grateful to the EPSRC for their financial support under grant EP/E036945/1 on the Modelling and Simulation of Intermittent Flows.

REFERENCES

1. Andreotti B, Douady S (1999). On probability distribution functions in turbulence. Part 1. A regularisation method to improve the estimate of a PDF from an experimental histogram. *Physica D* 132:111–132.
2. Akselvoll K, Moin P (1996). Large eddy simulation of turbulent confined coannular jets. *J. Fluid Mechanics* 315:387–411.
3. Babu P. Mahesh K (2005). Direct numerical simulation of passive scalar mixing in spatially evolving turbulent round jets. *AIAA Sci. Meeting,* 2005–1121.
4. Batchelor GK (1959). Small scale variation of convected quantities like temperature in turbulent fluid. *J. Fluid Mech.* 5:113–139
5. Bell JB, Colella P, Glaz HM (1989). A second order projection method for the incompressible Navier-Stokes equations. *J. Comput. Phys.* 85:257–283.
6. Becker HA, Hottel HC, Williams GC (1967). The nozzle fluid concentration field of the round turbulent jet. *J. Fluid Mech.* 30:285–301.
7. Birch AD, Brown DR, Dodson MD, Thomas JR (1978). The turbulent concentration field of a methane jet. *J. Fluid Mech.* 88:431–449.
8. Broadwell JE, Breidenthal RE (1982). A simple model of mixing and chemical reaction in a turbulent shear layer. *J. Fluid Mech.* 125:397–410.
9. Brancher P, Chomaz JM, Huerre P (1994). Direct numerical simulations of round jets: vortex induction and side jets. *Phys. Fluids* 6:1768–1773.
10. Boersma BJ, Brethouwer G, Nieuwstadt FTM (1998). A numerical investigation on the effect of the inflow conditions on the self-similar region of a round jet. *Phys. Fluids* 10:899–909.
11. Corrsin S (1943). Investigation of flow in an axially symmetrical heated jet of air. *NACA Wash. Wartime Report*, W-94.
12. Corrsin S, Uberoi MS (1950). Further experiments on the flow and heat transfer in a heated turbulent air jet. *NACA Rep.*, 998.
13. Corrsin S (1951). On the spectrum of isotropic temperature fluctuations in isotropic turbulence. *J. Appl. Phys.* 22:469–473.
14. Dahm WJA, Dimotakis PE (1985). Measurements of entrainment and mixing in turbulent jets. *AIAA 23rd Aerospace Sciences Meeting*, Paper 85-0056.
15. Dianat M, Yang Z, Jiang D, McGuirk JJ (2006). Large eddy simulation of scalar mixing in a coaxial confined jet. *Flow Turb. Combust*. 77:205–227.
16. Dowling DR, Dimotakis PE (1990). Similarity of the concentration field of gas phase turbulent jets. *J. Fluid Mech.* 218:109–141.
17. Frohlich J, Garcia-Villalba M, Rodi W (2008). Scalar mixing and large scale coherent structures in a turbulent swirling jet. *Flow Turb. Combust*. 80(1):47–59.
18. Garcia-Villalba M, Frohlich J, Rodi W (2006). Identification and analysis of coherent structures in the near field of a turbulent confined annular swirling jet using large eddy simulation. *Phy. of Fluids* 18:1–17.
19. Hussein HJ, Capp SP, George WK (1994). Velocity measurements in a high Reynolds number,momentum-conserving, axisymmetric, turbulent jet. *J. Fluid Mech*. 258:31–76.
20. Kempf A, Malalasekera W, Ranga Dinesh, KKJ, Stein O (2008). Large eddy simulation with swirling non-premixed flames with flamelet model: A comparison of numerical methods. *Flow Turb. Combust* 81:523–561.
21. Kirkpatrick MP, Armfield SW, Kent JH (2003a). A representation of curved boundaries for the solution of the Navier-Stokes equations on a staggered three-

dimensional Cartesian grid. *J. of Comput. Phy.*184:1–36.
22. Kirkpatrick MP, Armfield SW, Masri AR, Ibrahim SS (2003b). Large eddy simulation of a propagating turbulent premixed flame. *Flow Turb. and Combust* 70(1):1–19.
23. Kirkpatrick MP, Armfield SW (2008). On the stability and performance of the projection-3 method for the time integration of the Navier-Stokes equations. *ANZIAM Journal* 49:C559 –C575.
24. Kerstein AR (1990). Linear eddy modelling of turbulent transport, Part 3. Mixing and differential molecular diffusion in round jets. *J. Fluid Mech.* 216:411–435.
25. Leonard BP, Mokhtari S (1990). Beyond first order upwind: The ULTRA SHARP alternative for non-oscillatory steady-simulation of convection. *Int. J. Num. Meth. Eng.* 30:729–766.
26. Lubbers CL, Brethouwer G, Boersma BJ (2001). Simulation of the mixing of a passive scalar in a round turbulent jet. *Fluid Dy. Research* 28:189–208.
27. Malalasekera W, Ranga Dinesh KKJ, Ibrahim SS, Kirkpatrick MP (2007). Large eddy simulation of isothermal turbulent swirling jets. *Combust. Sci. Tech.* 179:1481–1525.
28. Oboukhov AM (1949). Structure of the temperature field in turbulent flows. *Izv. Ak. Nauk SSR. Geogr. Geophys* 13:58–69.
29. Panchapakesan NR, Lumley JL (1993). Turbulence measurements in axisymmetric jets of air and helium. Part 1. Air jet. *J. Fluid Mech.* 246:197–224.
30. Pierce C, Moin P (1998). Large eddy simulation of a confined coaxial jet with swirl and heat release, *AIAA* Paper no 98-2892.
31. Piomelli U, Liu J (1995). Large eddy simulation of channel flows using a localized dynamic model *Phy. Fluids* 7:839–848.
32. Ranga Dinesh KKJ, Kirkpatrick MP (2009). Study of jet precession, recirculation and vortex breakdown in turbulent swirling jets using LES. *Int. J. Comput. Fluids* 38:1232–1242.
33. Schefer RW, Dibble RW (2001), Mixture fraction field in a turbulent nonreacting propane jet. *AIAA J.* 39:64–72.
34. Scheffer RE, Kerstein AR, Namazian M, Kelly J (1994). Role of large-scale structure in a nonreacting turbulent CH4 jet. *Phys. Fluids* 6:652–661.
35. Smagorinsky J (1963). General circulation experiments with the primitive equations. *M. Weather Review* 91:99–164.
36. Van Kan JA (1986). Second order accurate pressure correction scheme fir viscous incompressible flow. *SIAM J. Sci. Stat. Comput.* 7:870–891.
37. Verzicco R, Orlandi P (1994). Direct simulations of the transitional regime of a circular jet. *Phys. Fluids* 6:751–759.
38. Warhaft, Z (2000). Passive scalars in turbulent flows. *Ann. Rev. Fluid Mech.* 32:203–240.
39. Wygnanski I, Fiedler HE (1969). Some measurements in the self preserving jet. *J. Fluid Mech.* 38:577–612.